Experimental energy-density flux characterization of ultrashort laser pulse filaments

Daniele Faccio[1,5], Antonio Lotti[1,5], Aidas Matijosius[2], Francesca Bragheri[4,5], Vittorio Degiorgio[4,5], Arnaud Couairon[3,5], Paolo Di Trapani[1,2,5]

[1]*CNISM and Department of Physics and Mathematics, Università dell'Insubria, Via Valleggio 11, IT-22100 Como, Italy*
[2]*Department of Quantum Electronics, Vilnius University, Saulėtekio Ave. 9, bldg.3, LT-10222, Vilnius, Lithuania*
[3]*Centre de Physique Théorique, CNRS, École Polytechnique, F-91128, Palaiseau, France*
[4] *Department of Electronics, University of Pavia, Via Ferrata 1, I-27100 Pavia, Italy*
[5]*Virtual Institute for Nonlinear Optics, Centro di Cultura Scientifica Alessandro Volta, Villa Olmo, Via Simone Cantoni 1, 22100 Como, Italy*

daniele.faccio@uninsubria.it

Abstract: Visualization of the energy density flux gives a unique insight into the propagation properties of complex ultrashort pulses. This analysis, formerly relegated to numerical investigations, is here shown to be an invaluable experimental diagnostic tool. By retrieving the spatio-temporal amplitude and phase we experimentally obtain the energy density flux within complex ultrashort pulses generated by filamentation in a nonlinear Kerr medium.

OCIS codes: (190.5940) Self-action effects; (320.2250) Femtosecond phenomena; (190.5890) Scattering, stimulated.

References and links

1. Y. Roichman, B. Sun, Y. Roichman, J. Amato-Grill, and D. G. Grier, "Optical forces arising from phase gradients," Phys. Rev. Lett. **100**, 013602 (2008).
2. A.C. Peacock and N. G. R. Broderick, "Guided modes in channel waveguides with a negative index of refraction," Opt. Express **11**, 2502–2510 (2003).
3. H. I. Sztul and R. R. Alfano, "The Poynting vector and angular momentum of Airy beams," Opt.Express **16**, 9411–9416 (2008).
4. E. Recami, "On localized X-shaped superluminal solutions to Maxwell equations," Physica A **252**, 586–610 (1998).
5. P. Polesana, M. Franco, A. Couairon, D. Faccio, and P. Di Trapani, "Filamentation in Kerr media from pulsed Bessel beams," Phys. Rev. A **77**, 043814 (2008).
6. D. Faccio, A. Averchi, A. Lotti, P. Di Trapani, A. Couairon, D. Papazoglou, and S. Tzortzakis, "Ultrashort laser pulse filamentation from spontaneous X Wave formation in air," Opt. Express **16**, 1565–1570 (2008).
7. D. Faccio, M. Clerici, A. Averchi, A. Lotti, O. Jedrkiewicz, A. Dubietis, G. Tamosauskas, A. Couairon, F. Bragheri, D. Papazoglou, S. Tzortzakis, and P. Di Trapani, "Few-cycle laser pulse collapse in Kerr media: the role of group velocity dispersion and X wave formation," Phys. Rev. A. **78**, 033826 (2008).
8. K. E. Oughstun, "Asymptotic description of pulsed ultrawideband electromagnetic beam field propagation in dispersive, attenuative media," J. Opt. Soc. Am. A **18**, 1704–1713 (2001).
9. A. S. Wyatt, I. A. Walmsley, G. Stibenz, and G. Steinmeyer, "Sub-10 fs pulse characterization using spatially encoded arrangement for spectral phase interferometry for direct electric field reconstruction," Opt. Lett. **31**, 1914–1916 (2006)

#108291 - $15.00 USD Received 3 Mar 2009; revised 3 Apr 2009; accepted 6 Apr 2009; published 30 Apr 2009

10. P. Gabolde and R. Trebino, "Self-referenced measurement of the complete electric field of ultrashort pulses," Opt. Express **12**, 4423–4429 (2004).
11. P. Bowlan, U. Fuchs, R. Trebino, and U. D. Zeitner, "Measuring the spatiotemporal electric field of tightly focused ultrashort pulses with sub-micron spatial resolution," Opt. Express **16**, 13663–13675 (2008).
12. C. Dorrer, E. M. Kosik, and I. A. Walmsley, "Direct space time-characterization of the electric fields of ultrashort optical pulses," Opt. Lett. **27**, 548–550 (2002).
13. F. Bragheri, D. Faccio, F. Bonaretti, A. Lotti, M. Clerici, O. Jedrkiewicz, C. Liberale, S. Henin, L. Tartara, V. Degiorgio, and P. Di Trapani, "Complete retrieval of the field of ultrashort optical pulses using the angle-frequency spectrum," Opt. Lett. **33**, 2952–2954 (2008).
14. A. Couairon and A. Mysyrowicz, "Femtosecond filamentation in transparent media," Phys. Rep. **441**, 47-189 (2007).
15. J. Trull, O. Jedrkiewicz, P. Di Trapani, A. Matijosius, A. Varanavičius, G. Valiulis, R. Danielius, E. Kucinskas, A. Piskarskas, and S. Trillo, "Spatiotemporal three-dimensional mapping of nonlinear X waves," Phys. Rev. E **69**, 026607 (2004).
16. D. Faccio, A. Matijosius, A. Dubietis, R. Piskarskas, A. Varanavičius, E. Gaizauskas, A. Piskarskas, A. Couairon, and P. Di Trapani, "Near- and far-field evolution of laser pulse filaments in Kerr media," Phys. Rev. E **72**, 037601 (2005).
17. M. A. C. Potenza, S. Minardi, J. Trull, G. Blasi, D. Salerno, A. Varanavičius, A. Piskarskas, and P. Di Trapani, "Three dimensional imaging of short-pulses," Opt. Commun. **229**, 381–390 (2004).
18. D. Faccio, P. Di Trapani, S. Minardi, A. Bramati, F. Bragheri, C. Liberale, V. Degiorgio, A. Dubietis, and A. Matijosius, "Far-field spectral characterization of conical emission and filamentation in Kerr media," J. Opt. Soc. Am. B **22**, 862–869 (2005).
19. J. R. Fienup, "Phase retrieval algorithms: a comparison," Appl. Opt. **21** 2758–2769 (1982).
20. R. Boyd, *Nonlinear Optics* (Academic Press, New York, 2002).
21. A. Zaïr, A. Guandalini, F. Schapper, M. Holler J. Biegert, L. Gallmann, A. Couairon, M. Franco, A. Mysyrowicz, and U. Keller, "Spatio-temporal characterization of few-cycle pulses obtained by filamentation," Opt. Express **15**, 5394–5405 (2007).
22. P. Di Trapani, G. Valiulis, A. Piskarskas, O. Jedrkiewicz, J. Trull, C. Conti, and S. Trillo, "Spontaneously generated X-shaped light bullets," Phys. Rev. Lett. **91**, 93904 (2003).
23. C. Conti, S. Trillo, P. Di Trapani, G. Valiulis, A. Piskarskas, O. Jedrkiewicz, and J. Trull,"Nonlinear electromagnetic X Waves, Phys. Rev. Lett. **90**, 170406 (2003).
24. A. Couairon, E. Gaizauskas, D. Faccio, A. Dubietis, and P. Di Trapani, "Nonlinear X-wave formation by femtosecond filamentation in Kerr media," Phys. Rev. E. **73**, 016608 (2006).
25. M. Kolesik, E. M. Wright, and J. V. Moloney, "Dynamic Nonlinear X waves for Femtosecond Pulse Propagation in Water," Phys. Rev. Lett. **92**, 2539011 (2004).
26. D. Faccio, M. A. Porras, A. Dubietis, F. Bragheri, A. Couairon, and P. Di Trapani, "Conical Emission, Pulse Splitting, and X wave Parametric Amplification in Nonlinear Dynamics of Ultrashort Light Pulses," Phys. Rev. Lett. **96**, 1939011 (2006).
27. D. Faccio, A. Averchi, A. Couairon, M. Kolesik, J. V. Moloney, A. Dubietis, G. Tamosauskas, P. Polesana, A. Piskarskas, and P. Di Trapani, "Spatio-temporal reshaping and X wave dynamics in optical filaments," Opt. Express **15**, 13079–13095 (2007).
28. J. Extermann, L. Bonacina, F. Courvoisier, D. Kiselev, Y. Mugnier, R. Le Dantec, Christine Galez, and J. P. Wolf, "Nano-FROG: Frequency Resolved Optical Gating by a nanometric object" Opt. Express **16**, 10405–10411 (2008).
29. P. Bowlan, P. Gabolde, A. Shreenath, K. McGresham, R. Trebino, and S. Akturk, "Crossed-beam spectral interferometry: a simple, high-spectral-resolution method for completely characterizing complex ultrashort pulses in real time," Opt. Express **14**, 11892–11900 (2006).
30. S. Mokhov and R. El-Ganainy, and D. N. Christodoulides, "Power circulation via negative energy-flux wormholes in optical nanowaveguides" Opt. Express **14**, 3255–3262 (2006).
31. H. S. Green and E. Wolf, "A scalar representation of electromagnetic fields," Proc. Phys. Soc. LXVI **66**, 1129–1137 (1953).
32. E. Wolf, "A scalar representation of electromagnetic fields: II," Proc. Phys. Soc. **74**, 269–280 (1959).

The energy flux defined through the Poynting vector is a fundamental quantity for describing the propagation properties of light. Examples of properties opening the way to applications range range from particle trapping through phase-gradients [1], light-traps in negative index waveguides [2], accelerating Airy beams [3] to X-wave propagation [4, 5, 6]. However, due to the intrinsic difficulty in experimentally measuring the energy density flux within tightly focused and complex pulses, these studies have so far been limited to numerical investiagtions. Usually defined as $\vec{S} = \vec{E} \times \vec{H}$, the energy flux must be re-written in terms

#108291 - $15.00 USD Received 3 Mar 2009; revised 3 Apr 2009; accepted 6 Apr 2009; published 30 Apr 2009

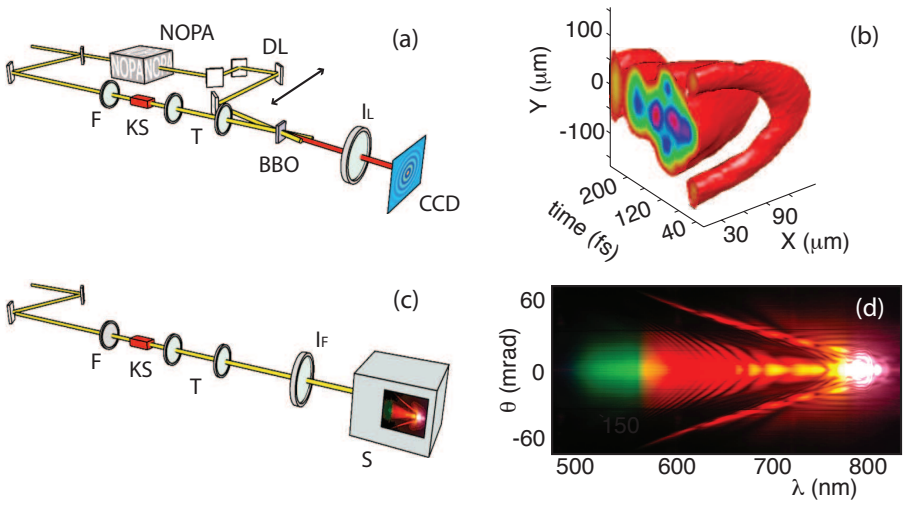

Fig. 1. (a) Experimental layout for the 3D tomography measurement: DL - delay line, F - focusing lens, KS - Kerr sample, T - imaging telescope, BBO - nonlinear BBO crystal for sum-frequency between laser pulse and 20 fs NOPA gate pulse, I_L - imaging lens, CCD - imaging plane with CCD camera. (b), the experimentally retrieved space-time intensity profile of the laser filament (40 mm in water). (c) Experimental layout for the angularly resolved spectrum with (d), the experimentally measured spectrum for the same filament pulse shown in (b). I_F - Fourier lens, S - imaging spectrometer.

of the sole electric field E if an experimental measurement of the flux is to be performed. An alternative approach to defining an energy flux vector starts from the propagation equation (see Appendix) for the electric field complex amplitude $u = |u|\exp(i\phi)$ and leads to an expression for the radial and temporal energy flux $J_r = (1/2ik_0)[u^*\partial u/\partial r - u\partial u^*/\partial r]$ and $J_t = -(k_0''/2i)[u^*\partial u/\partial t - u\partial u^*/\partial t]$, respectively. Substituting u in these relations we find $J \propto I\nabla\phi$, thus indicating the dominant role played by the phase gradient in determining the energy density flux. An associated phenomenon is the existence of optical forces that arise from phase gradients and are described by similar equations [1]. The problem of measuring the energy density or momentum flux is then reduced to that of measuring the pulse phase profile with sufficient precision to allow reconstruction of the phase gradient along the spatial and temporal coordinates. Furthermore if the laser pulse exhibits space-time coupling, i.e. the temporal profile depends on the transverse spatial coordinate, then the phase measurement technique must account for this coupling and should not treat (measure) the spatial and temporal profiles independently. Such situations occur very frequently or may even become the norm for pulses of very broad bandwidth as it is sufficient to focus a pulse to observe space-time coupling (even in the linear regime) [8]. Here we draw attention to the case of ultrashort laser pulse filaments. High power laser pulses indeed undergo self-focusing in nonlinear Kerr media: the collapse is eventually arrested by multiphoton absorption or higher order nonlinear processes and a filament forms, i.e. a tightly localized intensity peak that propagates sub-diffractively over many diffraction lengths. This peak is surrounded by a larger energy reservoir and it is the interaction between the two that sustains long range nonlinear propagation and allows one to foresee applications based on long distance nonlinear interaction or on the transport of high intensities over long paths [14]. Many of the features of pulse propagation within filaments, such as temporal compression and sub-diffractive propagation, are still a matter of discussion. Recent numerical studies have highlighted a clear X-shaped structure in the filament energy density flux which

#108291 - $15.00 USD Received 3 Mar 2009; revised 3 Apr 2009; accepted 6 Apr 2009; published 30 Apr 2009

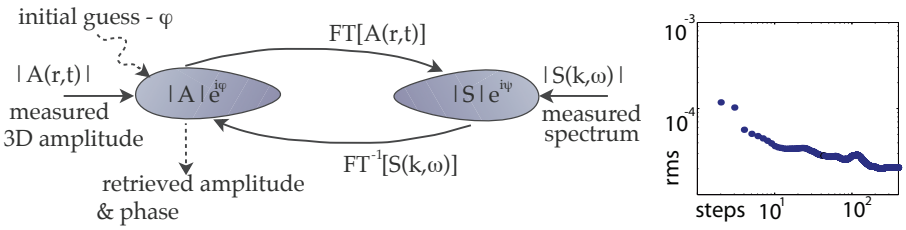

Fig. 2. Diagram of the Gerchberg-Saxton algorithm applied to the data in order to retrieve the pulse spatiotemporal amplitude and phase profile. An initial guess for the phase profile is superimposed on the measured 3D intensity profile. The spatiotemporal far-field spectrum is obtained by a Fourier transform whose amplitude is substituted with the measured one. An inverse Fourier transform gives a complex valued 3D near field profile in which the amplitude is replaced by the measurement. This process is iterated until convergence is obtained. The graph shows the the mean quadratic deviation between the retrieved and measured near-field intensity profiles over 400 steps.

is tightly connected to the appearance of the filament [5, 6, 7]. Here we extend these studies providing an experimental characterization of these complex pulses. In order to retrieve the energy density flux we must measure the pulse amplitude and phase. A number of techniques have been proposed for measuring the space-time amplitude and phase of complex ultrashort pulses each with its own advantages and drawbacks [9, 10, 11, 12, 13]. In principle any of these techniques may be applied to retrieve the filament amplitude and phase profile although we preferred to a technique, based on a near and far-field intensity measurement and phase retrieval through the Gerchberg-Saxton iterative error-reduction algorithm, as described below.

The characterization of the laser pulse filament is thus based on two separate measurements: the first is a 3D tomographic mapping of the pulse space-time intensity profile obtained by overlapping the pulse under study with a flat-top, 5 mm diameter (FWHM), 720 nm, 20 fs gate pulse, generated by a commercial noncollinear optical parametric amplifier (NOPA, Light Conversion Ltd.) on a 10 μm thick Beta Barium Borate (BBO) crystal [15, 16, 17]. The gate pulse spatial profile is flat over the spatial extension of the laser pulse (less than 500 μm so that the sum-frequency signal generated by the nonlinear BBO crystal reproduces the pulse spatial profile within the temporal window of the gate pulse. The thickness of the BBO crystal is chosen in order to have sufficient bandwidth ($\sim$ 300 nm) to convert the full spectrum (50 nm wide measured at FWHM) of the laser pulse. Changing the relative delay between the gate and laser pulse will therefore reconstruct the full space-time intensity profile of the laser pulse. The layout for this measurement is shown in Fig. 1(a). The filament is generated by focusing (f=50 cm) a 160 fs, 800 nm, 3.3 μJ laser pulse in a water cell whose length may be adjusted. The output facet of the cell is imaged onto the BBO crystal which in turn is imaged onto the CCD (16-bit camera, Andor Technologies) plane. The gate and laser pulses overlap on the BBO crystal with a small angle ($\sim$ 1 deg) so that a pinhole, placed after the BBO crystal may select only the noncollinear sum-frequency signal. In Fig. 1(b) we show an example of the reconstructed tomographic map of the laser pulse filament generated in 40 mm of water: the complexity of the pulse, characterized by multiple peaks and surrounding rings, is clear.

The second measurement consists of recording the angularly resolved (θ,λ) spectrum [18]. This is obtained by sending the spatial far-field of the filament, i.e. the intensity distribution in the focal plane of a lens, onto the input slit of an imaging spectrometer - the layout is shown in Fig. 1(c). The ouput (θ,λ) spectrum is then recorded with a CCD camera. Figure 1(d) shows a laser pulse filament spectrum measured after 40 mm of water, recorded with a color Nikon

#108291 - $15.00 USD Received 3 Mar 2009; revised 3 Apr 2009; accepted 6 Apr 2009; published 30 Apr 2009

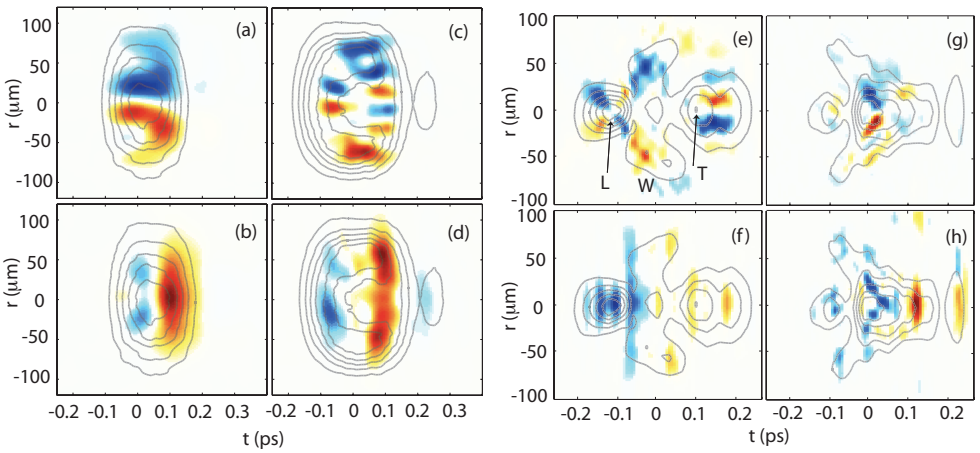

Fig. 3. Experimentally retrieved energy density flux profiles for an 800 nm, 160 fs laser pulse with a power 11 times the critical power for self-focusing in water. Blue indicates a negative (opposite to the axis direction), Red indicates a positive (same as the axis direction) flux. (a), (c), (e) and (g) show the normalized r-t distribution of transverse flux for the input focused pulse, for the pulse after 0 mm, 10 mm, 20 mm and 40 mm of nonlinear propagation in water, respectively. (b), (d), (f) and (h), for the same conditions, show the longitudinal fluxes. The grey contour plots show the pulse space-time intensity profile over 2 decades (0.4 decade spacing between each contour line). In (e), "L", "T" and "W" indicate the leading peak, the trailing peak and the central wings, respectively.

digital camera that highlights the colored conical emission, i.e. the extended tails propagating at off-axis angles. Recovery of the pulse phase profile was obtained using spectra recorded on a linearized 16-bit CCD camera, in order to avoid saturation in the high intensity regions and distortions due to the Nikon nonlinear CCD response. We note that the imaging spectrometer has an input slit which necessarily limits the (θ,λ) measurement to a single slice in the transverse plane: due to the azimuthal symmetry of the laser pulse filament this is sufficient information to recover the full space-time phase profile.

The problem of recovering the phase profile from intensity Fourier-transform pairs is well known in the field of spatial wave-front sensing: the phase profile is retrieved by combining the near and far field intensity measurements through an error-reduction (or Gerchberg-Saxton) algorithm [19]. Considering that our (r,t) and (θ,λ) measurements also form a Fourier transform pair, we simply generalize the error-reduction algorithm to the space-time domain. In more detail, phase retrieval is obtained via an iterative Gerchberg-Saxton algorithm in which the complex field is Fourier-transformed back and forth, each time substituting the relative measured (r,t) or (θ,λ) intensity profile (Fig. 2). The algorithm was first tested on a number of numerically generated test pulses, e.g. tilted pulses with various phase profiles, each time showing robust behavior and convergence to the correct phase profile. The algorithm was the run using measured data for a total of 400 iterations with an initial quadratic guess function for the phase profile. Convergence to similar results was obtained even by widely varying (by more than a factor 50) the input phase curvature although we finally present the results that effectively minimized the "error", i.e. the mean quadratic deviation between the retrieved and measured near-field intensity profiles. We note that the Gerchberg-Saxton algorithm is afflicted by an ambiguity in the sign of the retrieved phase, e.g. it cannot discriminate between a focusing or a defocusing Gaussian beam. This ambiguity can be removed if the sign of the phase is actually

#108291 - $15.00 USD Received 3 Mar 2009; revised 3 Apr 2009; accepted 6 Apr 2009; published 30 Apr 2009

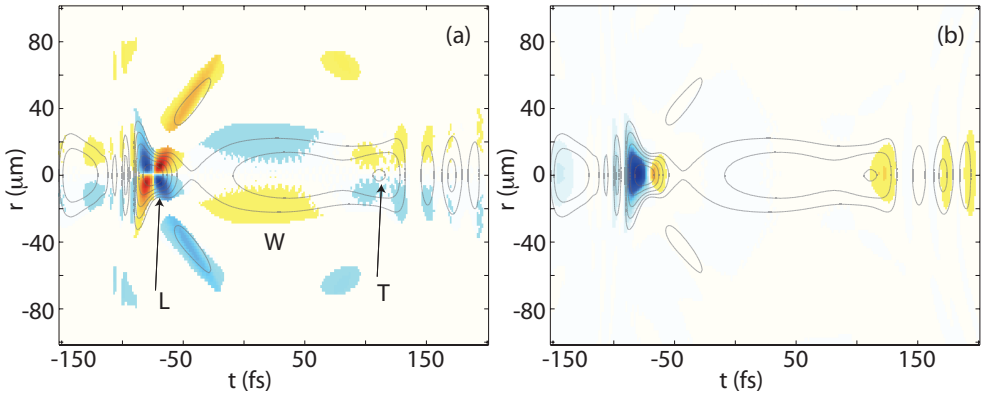

Fig. 4. Numerically simulated laser filament pulse and transverse flux after 40 mm of water. The input power and focusing conditions are chosen to match the experiment. The grey contour plots show the pulse space-time intensity profile over 4 decades (0.8 decade spacing between each contour line). "L", "T" and "W" indicate the leading peak, the trailing peak and the central wings, respectively. The main experimental features are reproduced, in particular the marked X-shaped flux associated to the main leading intensity peak.

known a priori. This is indeed the case for the input pulse ($z = 0$ cm) as it is focused into the medium with a lens and suffers initial linear positive dispersion. The same phase signs were applied also to the measurements at successive z. The good agreement between the measurements and the numerics at both a qualitative and quantitative level confirm the appropriateness of this choice.

Once the phase profile is retrieved the space-time energy-density flux, or equivalently the momentum flux, is retrieved using the formulas given above for J_r and J_t.

As a first example, we take the 3D tomographic measurements described in [16] for the input focused Gaussian laser pulse at $z = 0$ mm, i.e. in the absence of any nonlinear Kerr medium and for $z = 10$ mm propagation in water. For $z = 0$ mm, Figs. 3(a) and 3(b) show the normalized retrieved fluxes along the transverse direction r and along the longitudinal temporal coordinate t, respectively. The grey curves show the contours of the pulse space-time profile in logarithmic scale over 2 decades. Blue regions in the graph indicate a negative flux, red indicates a positive flux. The transverse flux clearly shows an inward flow toward the center of the pulse ($r = 0$) as expected for a linearly focusing pulse. The longitudinal flux shows two components, both flowing outward with respect to the center ($t = 0$) of the pulse as schematically indicated by the arrows. This flux is related to linear dispersion that leads to a temporal broadening of the pulse. Figures 3(c) and 3(d) show the same fluxes, in the reference frame of the input Gaussian pulse, for $z = 10$ mm. The input power is 11 times the critical power for self-focusing [20] and the nonlinear effects on the pulse are clearly visible. The transverse flux shows an inward flow due to self-focusing in correspondence to the leading region and to the outer regions ($|r| \geq 50$ μm) while the opposite outward flux carried by the trailing part and associated with the typical horn shape of the intensity profile is a clear signature of plasma defocusing arising from self-generated plasma [14, 21].

Using the same laser and input conditions as above, we performed further measurements and applied the technique to the fully formed filament ($z = 20$ mm and 40 mm propagation). At $z = 20$ mm propagation [Figs. 3(e), 3(f)] the pulse is split in two and the leading pulse (indicated with "L" in the figure) shows a marked X-shaped structure in the transverse flux distribution, i.e. a conical energy flux that is bringing energy from the surrounding reservoir

#108291 - $15.00 USD Received 3 Mar 2009; revised 3 Apr 2009; accepted 6 Apr 2009; published 30 Apr 2009

into the central intensity peak which is estimated (from the tomography measurements) to have a width of approximately 10 μm. The trailing pulse (indicated with "T" in the figure) on the other hand is still clearly affected by plasma defocusing and shows a marked outward flux. Furthermore we note the presence of an off-axis ring centered around t=0 (indicated with "W" in the figure) that is focusing toward the pulse axis. The conical X-shaped transverse-flux is still clearly visible after 40 mm propagation, even if the energy has recombined toward the pulse center. These results strongly support the presence of spontaneously formed nonlinear X-waves [22, 23, 24] and the interpretation of filamentation in terms of a dynamical interaction (splitting and refocusing) of nonlinear X-waves [25, 26]. X-waves are a particular class of non-diffractive and non-dispersive wave-packets that are characterized by a conical energy flux and indeed exhibit an X-shaped energy density flux profile in the near-field [4]. The transverse flux of the spontaneously formed X-waves in filamentation in condensed [5] and gaseous media [6] has been investigated numerically with results very similar to our experimental measurements. In Fig. 4 we show a numerically simulated laser filament intensity with its transverse and longitudinal flux distribution using the same experimental input conditions obtained with a model described in detail elsewhere [14]. The leading (L) and trailing peak (T) are separated by 200 fs in both the numerics and the experiments. In Fig. 4(a) the X-shaped flux associated to the leading peak and the outward flux associated to the trailing peak are clearly visible along with the inward flux around t=0 (W) in close agreement with the experimental measurement, Fig. 3(e). Furthermore, the numerical longitudinal flux Fig. 4(b) also shows similar features to the experiment, Fig. 3(f) with opposite flux directions on the leading and trailing peaks.

In conclusion we have experimentally retrieved the energy density flux within ultrashort laser pulse filaments. The flux shows a clear X-shaped profile that is reproduced also in numerical simulations and strongly supports the idea of spontaneous X-wave formation within filaments. The same approach proposed here may be applied to other situations and depending on the complexity of the pulse, other phase retrieval methods may also be adequate. In particular recent advances in frequency resolved optical techniques [28] and interferometric [29] methods applied to tightly focused or even to the nano-scale regime give promise of experimentally measuring the energy density flux in nano-waveguides [30] or scattering and trapping of nanometric particles.

Appendix

The energy density flux used was derived starting from the propagation equation for the electric field complex amplitude u in the slowly varying envelope approximation is

$$\frac{\partial u}{\partial z} = \frac{i}{2k_0}\nabla_\perp^2 u - i\frac{k_0''}{2}\frac{\partial^2 u}{\partial t^2} + N(u) \tag{1}$$

where k_0 is the wave-vector and k_0'' is the second order derivative with respect to frequency, both evaluated at the carrier frequency ω_0 and $N(u)$ is a nonlinear term which for high intensity pulses describes the effects of Kerr nonlinearity, nonlinear absorption, plasma generation etc. [14]. Multiplying Eq. (1) by the complex conjugate u^* and summing member by member with the relative conjugate equation and assuming azimuthal symmetry, one obtains a continuity equation for the current of the energy density J. Projecting onto the radial coordinate r and the temporal coordinate t, J may be written as

$$J_r(r,t) = \frac{1}{2ik_0}\left[u(r,t)^*\frac{\partial u(r,t)}{\partial r} - u(r,t)\frac{\partial u(r,t)^*}{\partial r}\right] \tag{2}$$

$$J_t(r,t) = \frac{k_0''}{2i}\left[u(r,t)^*\frac{\partial u(r,t)}{\partial t} - u(r,t)\frac{\partial u(r,t)^*}{\partial t}\right] \tag{3}$$

#108291 - $15.00 USD Received 3 Mar 2009; revised 3 Apr 2009; accepted 6 Apr 2009; published 30 Apr 2009

In the Lorenz gauge the electric field is related to the vector potential A, $u = -\partial A/\partial t$. In the limit in which the vector amplitude varies slowly on the time scale of an oscillation of the carrier frequency ω, i.e. $E = i\omega A$, Eq. (2) coincides with the expression obtained directly from the time averaged Poynting vector while Eq. (3) represents its generalization along the temporal coordinate. We note that these relations coincide with the original equations first derived by H.S. Green and E.Wolf [31, 32]. Finally, writing $u = |u|\exp(i\phi)$ so that the pulse intensity is $I = |u|^2$and substituting for example in Eq. (2) we obtain $J_r = -(1/k_0)I(r)\nabla\phi(r)$. Strictly speaking Eqs. (2) and (3) are valid within the limits of the approximations used to derive Eq. (1), in particular the paraxial approximation. Future work will be dedicated to the details and implications of these approximations.

Acknowledgments

The authors acknowledge G. Tamosauskas and O. Jedrkiewicz for technical support and financial support from the Consorzio Nazionale Interuniversitario per le Scienze Fisiche della Materia (CNISM), project INNESCO and from MIUR project RBIN04NYLH. PDT acknowledges support from the Marie Curie Chair project STELLA MEXC-CT-2005-025710.

#108291 - $15.00 USD Received 3 Mar 2009; revised 3 Apr 2009; accepted 6 Apr 2009; published 30 Apr 2009